RSC Advances

ROYAL SOCIETY OF **CHEMISTRY**

www.rsc.org/advances

Investigation on the microstructure of as-deformed NiCr microwires

by TEM

X.W. Zhou[a,b], Y.D. Qi[b,c], X.D. Liu[b], J.J. Wei[a1], W.D. Wu[a,b]

[a] Institute of Atomic and Molecular Physics, Sichuan University, Chengdu 610065, China

[b] Research Center of Laser Fusion, China Academy of Engineering Physics, Mianyang 621900,China

[c]State Key Laboratory Cultivation Base for Nonmetal Composites and Functional Materials, Southwest University of

Science and Technology, Mianyang 621010, China

Abstract: Ultra-fine NiCr (80/20 wt.%) wires with nanocrystalline (nc) and diameters that range from 21 μm to 25 μm were fabricated using cold-drawing method. The engineering strains were 8.8%, 17.3%, 26.4%, 36.1%, and 46.6%. The microstructures of the drawn direction and wire cross-section were characterized using transmission electron microscopy (TEM). Two thinning preparation techniques were used in preparing TEM specimens. Grain size was approximately 3 nm to 20 nm. The deformed microstructures include amorphous GB, crystal GB, edge dislocations, and twins. Amorphous boundaries may produce by phase transition or dislocation pile-up. Several edge dislocations existed at the grain boundaries (GBs) and grain interior. Twinning deformation microstructures were found in cross-sections with asymmetrical relationship. The possible deformation mechanism for the formation of the microstructure is discussed.

Keywords: NiCr microwire, cold-drawing, microstructure, Z-pinch, TEM

1. Introduction

In the past few decades, a fact has been widely verified that metal wire-arrays are efficient generators of soft x-ray output power and energy in Z-pinch experiments [1-4]. The alloy wires with the similar line quality can produce high power Z-pinch implosions [5, 6]. Actually, the microstructure of micrometer-sized metallic wire is a key factor for the electrical current in the plasma to generate a magnetic pressure [7, 8].

Nickel-chrome (NiCr) alloy is one of the most important materials in Z-pinch experiments [9] due to the excellent corrosion-resistance properties in nature and very similar radiated conditions. Usually, the NiCr wires are purchased on the market

---

[1] **Corresponding author. Tel.:+86 816 2480872; fax: +86 816 2490535**
   E-mail address:xiuwenzhou@caep.cn (X. W. Zhou).

and prepared by drawing machine. In order to meet the needs of Z-pinch experiments, the diameters of NiCr wires should be decreased from above 20μm to needed size of 10μm to 20μm by cold-drawing method, which leads to the changes of the physical properties and microstructures [10, 11].

It is very important to understand deformation mechanisms from microstructures [12, 13]. The relationship between the microstructure and properties of NiCr ultra wire is worthy to establish for engineering application. However, it is difficult to prepare NiCr wire thin specimens for analyzing the microstructure because NiCr is a micrometer wire and a very hard metal. The mainly method of preparing TEM specimens is thinning preparation techniques published by Springer [14]. But some details must be improved for adapting to special metal wires. K. Noguchi et al. reported two methods to prepare thin specimens with the drawn direction cross-section (D. D. cross-section) and wire cross-section (T. D. cross-section) [15], respectively. There are two challenges that have to overcome in NiCr thin sample preparation. One is that NiCr wire is difficult to be cut using of the ultra-microtome relative to Au wire. The other is the additional deformation of samples can't be eliminated using two Cu tube method in cold-rolling process. In addition, there are no previous references in investigation on the microstructure of NiCr alloy ultra wires with nanocrystalline grain.

In this paper, the Ni80Cr20 (Ni20Cr) microwires were prepared by cold-drawing method and the High Resolution Transmission Electron Microscopy (HRTEM) was employed to examine their structures of GBs, including drawn direction and wire cross-section to determine the effects of grain boundaries on the deformation mechanisms.

2. Experimental

2.1 Sample fabrication

The Ni20Cr alloy with face-centered cubic structure used in this study possessed the following chemical composition: Ni, 20.037% Cr, 1.037% Si, 0.194% Mn, 0.141% Fe, 0.101% Ti, 0.087% Al, and 0.023% Cu (wt. %). Specimens were prepared by cold-drawing from the as-received microwire with a diameter of 25.6 μm through

one die in one pass. The as-deformed samples with diameters of 24.54, 23.64, 22.77, 21.94, and 21.14 μm exhibited engineering strains of 8.8%, 17.3%, 26.4%, 36.1%, and 46.6% ($\varepsilon = \left(l_1 - l_0 \right) / l_0 = r_0^2 / r_1^2 - 1$), respectively. Here l_0 and r_0 is the original length and radius, respectively. Where l_1 and r_1 is the current length and radius, respectively. The latter two samples were used to analyze the microstructure of the D. D. cross-section and T. D. cross-section by TEM.

2.2 Preparation of thin specimen

The microstructure of deformed Ni20Cr microwire was obtained by viewing flat and thin (<10 nm) specimens under TEM. The preparation technique of Ni20Cr specimens parallel to the D. D. cross-section was different form Noguchi's method. Microwires were fixed between two Cu sample holders by using the glue, the outer and inner diameters being 3 and 1 mm, respectively. Gun voltage and current of ion thinning were 5 kV and 2 mA, respectively. We fixed the angle α between wire and beam and rotate the specimen holder (angle β). The schematic diagram and geometry used are shown in Fig. 1. Angle α was set to approximately ±6° out of the specimen surface plane. The beams polished both faces of the specimen simultaneously. Angle β was set to approximately 30° by rotating the specimen from the normal direction of specimen surface plane.

Specimens of the T. D. cross-section were made by similar techniques as the film thinning preparation, including embedding, wire sawing, mechanical polishing, and dimpling. A schematic of the method is shown in Fig. 2. Samples were placed on the Si substrate parallel to each other by using the glue. Then it was hot glued to two pieces of Si support, with parameters of 120 °C and 2 h. The specimen thickness was mechanically polished from approximately 3 mm to 60 μm by abrasion. After being dimpled, the thickness of NiCr thin specimens enter zone is 20 μm to 30 μm. The specimens were thinned using the ion beam with parameters of D. D. cross-section for approximately 2.5 h.

3. Results and discussion

3.1 Deformed microstructure of D. D. cross-section

The microstructure of the Ni20Cr wire D. D. cross-section with a diameter of 21.14 μm was characterized using TEM. Thin specimen was prepared through the method as shown in Fig.1. The structures were removed by fast Fourier transforming (FFT) and inverse FFT processing, as shown in Fig. 3. The regions of Fig.3 (a)-Fig.3 (c) are the adjacent area with the same zone.

In Fig.3, there are eight grains marked A-F, H and I. Eleven GBs exist marked GB1- GB11, respectively. We can determinate GB3-GB5, GB8 and GB9 are crystal GBs maintaining right up to the boundary. We used two lines and two points to express the relationship of grains C and E, which are marked *a*, *a'*, *b*, and *b'*. Atoms of grain C intersect with line *a* at point a', twinning with the atoms of grain E by line *a*. Atoms of grain E intersect with line *b* at point *b'*, twinning with the atoms of grain C by line *b*. The twinning angle is approximately 141°. As is evidently observed from the TEM images, the GB between grains C and E is with the marked symmetrical structure. Twinning is an alternate mode of plastic deformation and is observed in conventional fcc metals and alloys with low stacking fault energy. When extreme deformation conditions are imposed, twins can be observed in fcc metals and alloys with relatively high stacking fault energy. The result agrees with several experimental observations and computations.

GB1, GB2, GB6, GB7, GB10 and GB11 are amorphous GBs (or generally called an "extended disordered region" or "randomly arranged atom"). The observation supports earlier postulates that stated the existence of an amorphous layer and is similar with Schuh's experimental observation. There are two possible reasons to explanation for this phenomenon. The first possible reason is slip dislocations plug product in grain boundary in the deformation processing. The result leaded to form substructures of amorphous GBs. The second possible reason is phase transitions had taken place in Ni20Cr alloy. B. Straumal reported phase transitions in metallic alloys driven by the high pressure torsion [12, 13]. Their results reveal the severe plastic deformation is equivalent to the heat treatment at a certain elevated temperature (effective temperature). The effective temperature is about 30□ to 1450□ in different alloy systems and components. It leads to phase transformations

e.g. amorphization, nanocrystallization, dissolution and decomposition, and so on. On the condition of traditional engineering strain, in the first zone (0 < time < 130 s), the drawing stress and the temperature increase from 0 to 310 MPa and from 15▯ to 50▯, respectively. In the second zone (130 s < time < 840), the drawing stress and the temperature increase progressively varying from 310 to 435 MPa and from 50▯ to 68▯, respectively [16]. In addition, Wright demonstrated the impact of drawing temperature on the microstructure of copper wire [17]. In our condition of abnormal engineering strain, the drawing stress and the temperature increase as high as a few times the former. It may result in amorphous GBs forming.

There are several distortion zones marked Arabic numeral in Fig.3 (a) and marked white line in Fig.3 (b) and Fig.3 (c). Edge dislocations exist in these zones. With distortion zones increasing, amorphous GBs form and grain are refined. The structure of region A1 in Fig. 3 (c) was processed by FFT, masked and inverse FFT, as shown in Fig. 3 (d). The (111) and $\left(11\overline{1}\right)$ lattice planes were observed. The grain exhibits a $\left[\overline{2}20\right]$ component. The observation is similar with Dudova's experimental observation by severe plastic deformation [18]. According to his report, the microstructure of the Ni–20Cr alloy strained to ε = ~6.5 included the (111) and $(11\overline{1})$ lattice planes, as well as the grain-contained dislocations at the GB and in the grain interior.

Above-mentioned zones are traced back to the image of D. D. cross-section are presented in Fig.4. Several evident boundaries are marked with a white profile. Grain size ranges from 5 nm to 20 nm. Moreover, grains exhibit an irregular shape, as well as the D. D. elongation of approximately 1.5 times to 10 times toward the vertical direction.

3.2 Deformation microstructure of T.D. cross-section

The results of TEM observation and selective area electron diffraction (SAED) of the wire cross-section are shown in Fig.5. The thin specimen was prepared from Ni20Cr wire with the diameter of 21.14 μm through the method as shown in Fig.2.

The SAED pattern indicates that the sample includes (111), (220), (311), and (420) crystal planes at the circle zone of SAED1, as well as the (111), (200), (220), and (311) crystal planes at the circle zone of SAED2. The appearance of the SAED pattern indicates that the specimen is polycrystalline with different orientations. From the patterns of SAED1 and SAED2, we can observe differences. In SAED1, (420) and distorted (311) crystal planes exist without (200). Distorted crystal planes may accord several distortion zones in Fig.1. However, the opposite result is observed in SAED2. As is evident in the results, the nature and distribution of nanocrystal grains vary in wire cross-section. Form the SAED pattern, we can observe the number of (220) and (111) lattice planes is more than other lattice planes. But the true proportion of lattice planes need to statistics the grain orientation in all range by electron back-scattered diffraction (EBSD).

Fig.6 shows the lattice plane and dislocation configuration of the SAED2 region in Fig.5. The microstructure, including (200) and (111) lattice planes, was observed. The structures of Fig.6 (a)-(c) were vanished by FFT, masked and inverse FFT processing, showing in Fig.6 (d)-(e). From the image, we can observe that edge dislocations, which are marked by white symbols in the image, exist at the grain interior. In the SAED2 region, there are some distorted crystal planes as shown in Fig.6 (c). It may be (311) crystal planes according to the SAED pattern. This result is identical to Dudova's observation [18]. According to his report, the microstructure of the Ni–20%Cr alloy strained to $\varepsilon = {\sim}2$ and $\varepsilon = {\sim}3$ included (200) and $(11\bar{1})$ lattice planes, as well as the grain-contained dislocations at the GB and in the grain interior.

Fig. 7 shows SAED and deformation twinning of the Ni20Cr alloy strained at $\varepsilon = 36.1\%$ in the wire cross-section. As seen in the SAED pattern, (110), (111), (200), (220), (311), and (222) lattice planes of Ni are observed as shown in Fig.7 (a) (top right corner). The presence of twinning reaction and an inhomogeneous distribution of twins were characterized in the wire cross-section. The relationship of deformation twinning of grains A, B, and A' (i.e., grain A) is indicated by several white lines as shown in Fig. 7 (b). We used three groups of lines to express the lattice

planes of each grain in the analysis plane, such as "line *a*, line *b*, line *c*," "line <*a*>, line <*b*>, line <*c*>," and "line *a'*, line *b'*, line *c'*." Evidently, line *a* is parallel to line *a'* (i.e., *a*), which is similar with line *b* to line *b'*. The orientation of grain A is the same as that of grain A'. Hence, we used grain A and the corresponding lines to replace grain A' and relevant lines. Grain B exists between grains A and A'. Line <*c*> is parallel to lines *c* and *c'*. However, lines <*a*> and *a*, as well as lines <*b*> and *b*, are unparallel. The twinning relationship exists between grains A and B, as well as between grains B and A'. The twinning angle is approximately 146°, which is slightly different from the twinning angle of approximately 141° in the D. D. cross-section.

It is clear that the edge dislocations exist in the grain interior. Four GBs exist marked GB1- GB4, respectively. We can determinate that all of them are crystal GBs maintaining right up to the boundary. GB1-GB3 shows the movement of GB in the process of twin deformation.

3.3 Deformation mechanism

These deformed microwires usually possess low ductility. Elongation-to-failure values strained to ε = 36.1% and ε = 46.6% are approximately 2.1% and 1.9%, respectively. Grain size ranges from 5 nm to 20 nm. Grains exhibit an irregular shape, along the D. D. elongation of approximately 1.5 times to 10 times toward the vertical direction. According to Wang's perspective [19], normal dislocation slip ceased to control plastic deformation when grain sizes were below ~30 nm. In partial dislocation-mediated processes, GB sliding will be predominant for grain sizes below ~10 nm.

Notably, the deformed structures of the Ni20Cr microwire included dislocation, twinning, and misfit from previous sections. Several dislocations were found in the grain interior. Several dislocations also existed at the boundary and maintained right up to adjacent grain. Amorphous boundaries act as sources and sinks for dislocation. The effects of dislocations and amorphous GB include stress-relief mechanism, either as GB sliding or twinning deformation. Therefore, GB sliding and twinning are the deformation mechanisms of nc Ni20Cr alloy at room temperature and under quasi-static strain rate. Twinning deformation is one of the factors that promoted

strain hardening.

4. Conclusions

In summary, the two mentioned methods were effective in preparing the TEM cross-section specimen of ultra-fine Ni20Cr wires. The deformed microstructures include amorphous GB, crystal GB, edge dislocations, and twins. Amorphous boundaries may produce by phase transition or dislocation pile-up. Edge dislocations exist in GB and grain interiors. Twinning relationships in both cross-sections are characterized with angles of approximately 141° and 146°, respectively. GB sliding and twinning are the deformation mechanisms of nc Ni20Cr at room temperature and under a quasi-static strain rate.

Acknowledgements

References

[1] M. G. Haines, A review of the dense Z-pinch, Plasma Physics and Controlled Fusion, 2011, 53(9):093001.

[2]D. J. Ampleford, S. B. Hansen, C. A. Jennings, B. Jones, C. A. Coverdale, A. J. Harvey-Thompson, G. A. Rochau, G. Dunham, N. W. Moore, E. C. Harding, M. E. Cuneo, Y.-K. Chong, R. W. Clark, N. Ouart, J. W. Thornhill, J. Giuliani, J. P, Apruzese. Opacity and gradients in aluminum wire array z-pinch implosions on the Z pulsed power facility, Physics of Plasmas, 2014, 21(3):031201.

[3]D. J. Ampleford, B. Jones, C. A. Jennings, S. B. Hansen, M. E. Cuneo, A. J. Harvey-Thompson, G. A. Rochau, C. A. Coverdale, A. R. Laspe, T. M. Flanagan, N. W. Moore, D. B. Sinars, D. C. Lamppa, E. C. Harding, J. W. Thornhill, J. L. Giuliani, Y.-K. Chong, J. P. Apruzese, A. L. Velikovich, A. Dasgupta, N. Ouart, W. A. Sygar, M. E. Savage, J. K. Moore, R. Focia, T. C. Wagoner, K. L. Killebrew, A. D. Edens, G. S. Dunham, M. C. Jones, P. W. Lake, D. S. Nielsen, M. Wu, A. L. Carlson, M. D. Kernahan, C. R. Ball, R. D. Scharberg, T. D. Mulville, E. W. Breden, C. S. Speas, G. Olivas, M. A. Sullivan, A. J. York, D. W. Justus, J. C. Cisneros, T. Strizic, J. Reneker, M. Cleveland, M. P. Vigil, G. Robertson, D. Sandoval, C. Cox, A. J. Maurer, D. A. Graham, N. B. Huynh, S. Toledo, L. P. Molina, M. R. Lopez, F.

W. Long, G. R. McKee, J. L. Porter, M. C. Herrmann, Contrasting physics in wire array z pinch sources of 1-20 keV emission on the Z facility, Physics of Plasmas.2014, 21(5):056708.

[4] X. Q. Gao, W.C. Hu, Y. S. Gao, Preparation of ultrafine tungsten wire via electrochemical method in an ionic liquid, Fusion Engineering and Design, 2013, 88 (1):23-27.

[5]D. B. Sinars, R. D. McBride, S. A. Pikuz, T. A. Shelkovenko, D. F. Wenger, M. E. Cuneo, E. P. Yu, J. P. Chittenden, E. C. Harding, S. B. Hansen, B. P. Peyton, D. J. Ampleford, C. A. Jennings, Investigation of High-Temperature Bright Plasma X-ray Sources Produced in 5-MA X-Pinch Experiments, Physical Review Letters, 2012, 109(15):155002.

[6]D. L. Xiao, N. Ding, C. Xue, J. Huang, Y. Zhang, C. Ning, S. K. Sun, Increasing the K-shell yield of line radiation in Z-pinch implosions using alloyed Al/Mg wire-arrays, Physics of Plasmas, 2013, 20(1):013304.

[7]R. A. Vesey, M. C. Herrmann, R. W. Lemke, M. P. Desjarlais, M. E. Cuneo1, W. A. Stygar, G. R. Bennett, R. B. Campbell, P. J. Christenson, T. A. Mehlhorn, J. L. Porter, S. A. Slutz, Target design for high fusion yield with the double Z-pinch-driven hohlraum, Physics of Plasmas, 2007, 14(5):056302.

[8]J.L. Remo, M.D. Furnish, Analysis of Z-pinch shock wave experiments on meteorite and planetary materials, International Journal of Impact Engineering, 2008, 35(12):1516–1521.

[9] T. A. Shelkovenko, D. B. Sinars, S. A. Pikuz, and D. A. Hammer, Radiographic and spectroscopic studies of X-pinch plasma implosion dynamics and x-ray burst emission characteristics, Physics of Plasmas, 2001, 8(4):1305-1318.

[10]Y.J. Li, P. Choi, S. Goto, C. Borchers, D. Raabe, R. Kirchheim, Evolution of strength and microstructure during annealing of heavily cold-drawn 6.3 GPa hypereutectoid pearlitic steel wire, Acta Materialia, 2012, 60(9):4005–4016.

[11]F. Fang, X. J. Hu, S. H. Chen, Z. H. Xie, J. Q. Jiang, Revealing microstructural and mechanical characteristics of cold-drawn pearlitic steel wires undergoing simulated galvanization treatment, Materials Science and Engineering: A, 2012, 547:51–54.

[12] B. B. Straumal, X. Sauvage, B. Baretzky, A. A. Mazilkin, R. Z. Valiev, Grain boundary films in Al－Zn alloys after high pressure torsion, 2014,70:59-62.

[13] B. Straumal, A. Korneva, P. Zieba, Phase transitions in metallic alloys driven by the high pressure torsion, 2014,14:242-249.

[14]J. Ayche, L. Beaunier, J. Boumendil, G. Ehret, D. Laub, Sample preparation handbook for transmission electron microscopy, Springer press, 2009 (chapter 3).

[15]K. Noguchi, M. Araki, Y. Ohno, The preparation of transmission electron microscopy specimens of as-drawn gold wire, Acta Mater. 51 (2003) 5743-5774.

[16] A. Haddi, A. Imad, G. VegaK, Analysis of temperature and speed effects on the drawing stress for improving the wire drawing process, Materials and design, 32 (2011) 4310-4315.

[17] A. E. Domiaty, S. Z. Kassab, Temperature rise in wire-drawing, Materials processing technology, 83 (1998) 72-83.

[18] N. Dudova, A. Belyakov, R. Kaibyshev, Recrystallization behavior of a Ni-20%Cr alloy subjected to severe plastic deformation, Materials science and engineering A 543 (2012) 164-172.

[19] Y. M. Wang, E. Ma, Three strategies to achieve uniform tensile deformation in a nanostructured metal, Acta Mater,52 (2004) 1699-1709.

Figure captions

Fig.1. Schematic diagram of preparing thin specimen in drawn direction cross-section

Fig.2. Schematic diagram of preparing thin specimen in wire cross-section
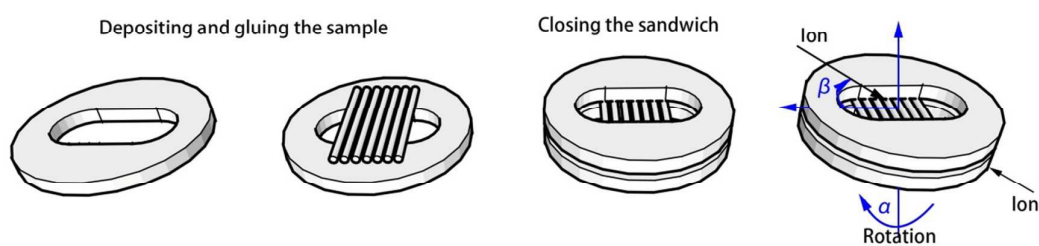
Fig.3. Deformed structures of Ni20Cr wire with engineering strain 46.6% in the D. D. cross-section

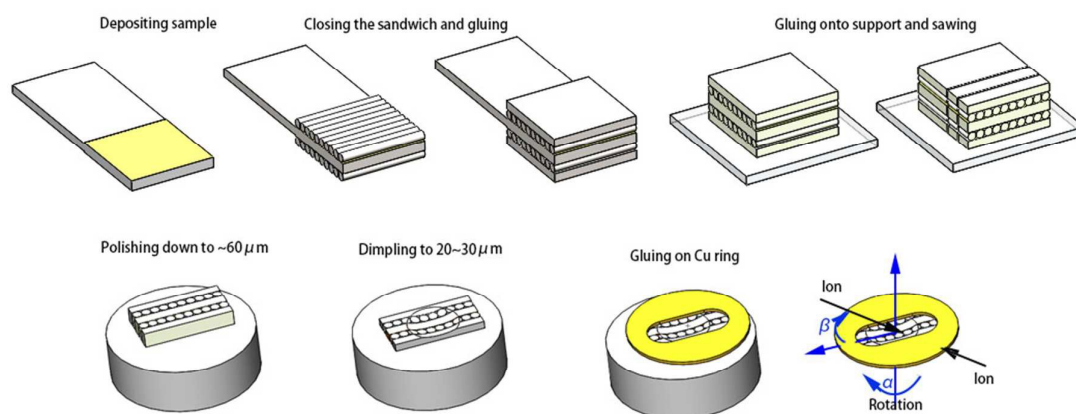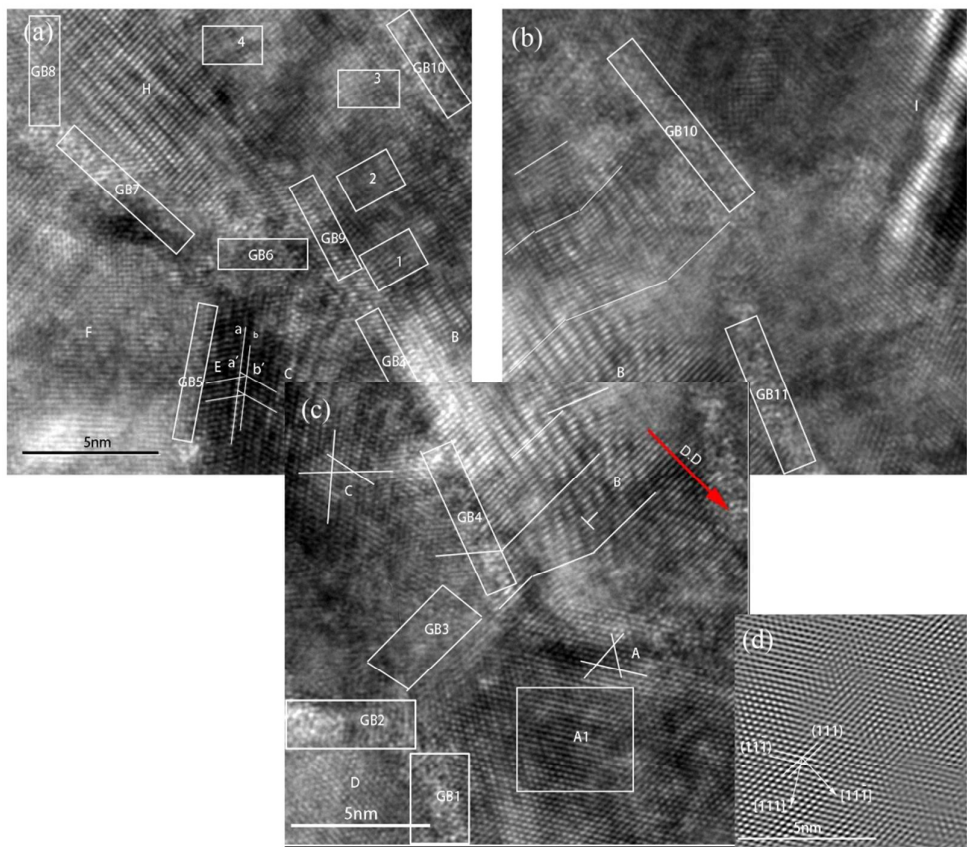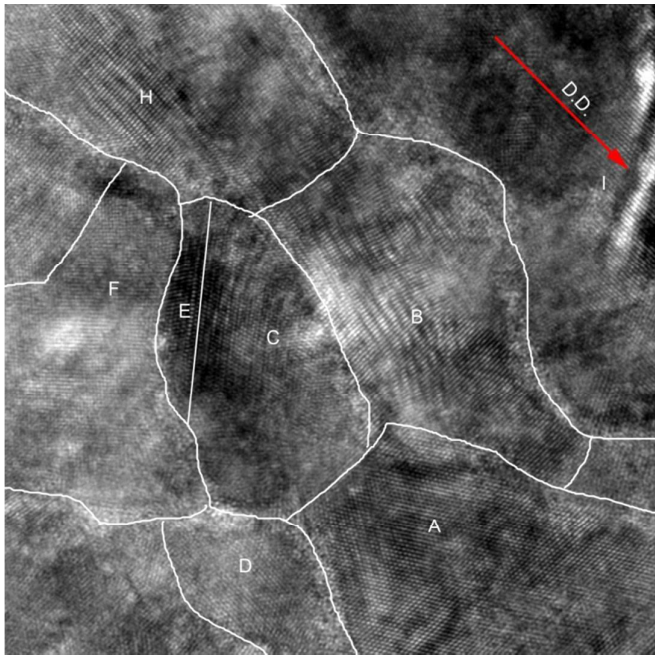**Fig.4.** TEM micrograph of Ni20Cr wire with engineering strain 46.6% in the D. D. cross-section

Fig.5. SEAD patterns of Ni20Cr wire with engineering strain 46.6% in the T. D. cross-section

Fig.6. Deformed structures and dislocation configuration of Ni20Cr wire with engineering strain 46.6% in the T. D. cross-section

Fig.7. SAED patterns and deformation twin of Ni20Cr wire with engineering strain 36.1% in the T. D. cross-section

Fig.1. Schematic diagram of preparing thin specimen in drawn direction cross-section

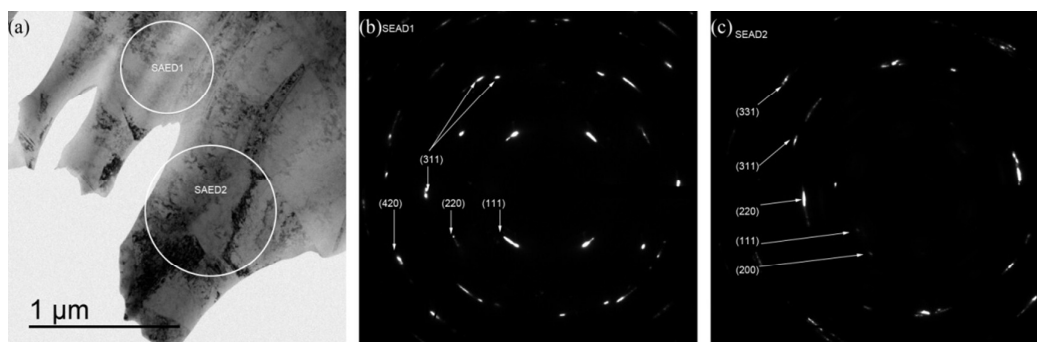**Fig.2.** Schematic diagram of preparing thin specimen in wire cross-section

Fig.3. Deformed structures of Ni20Cr wire with engineering strain 46.6% in the D. D.
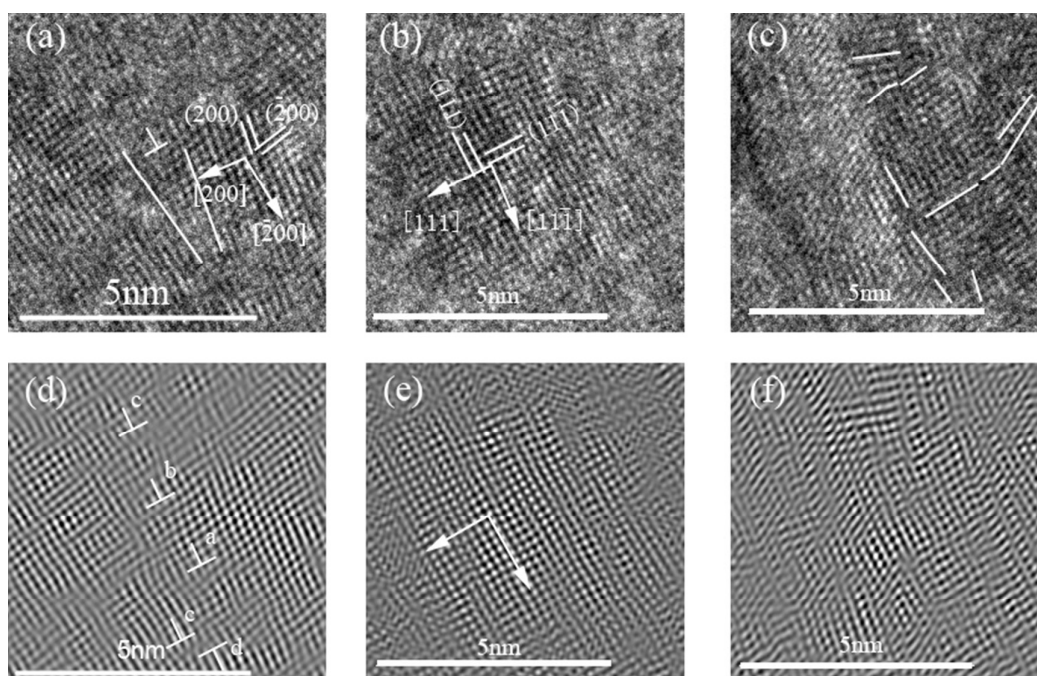
cross-section

Fig.4. TEM micrograph of Ni20Cr wire with engineering strain 46.6% in the D. D.
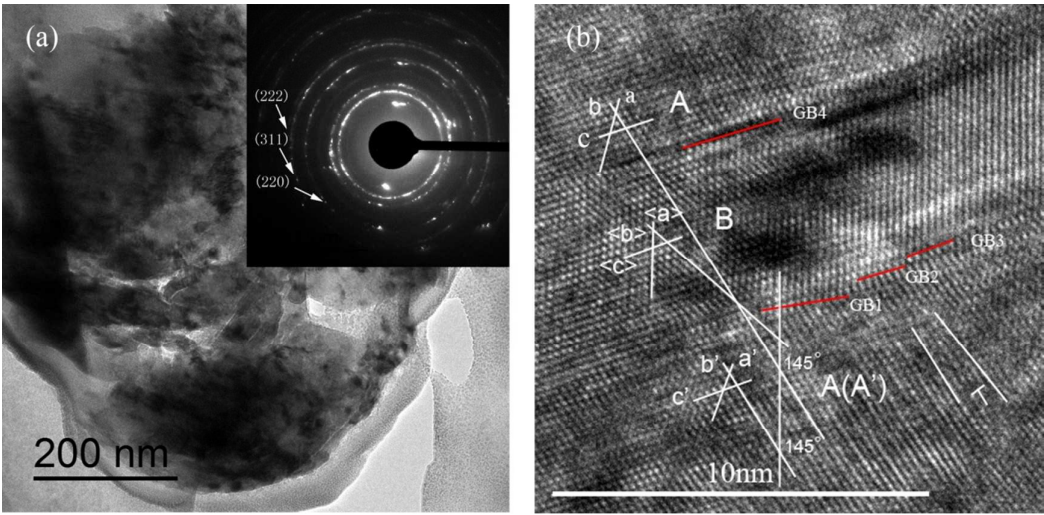
cross-section

Fig.5. SEAD patterns of Ni20Cr wire with engineering strain 46.6% in the T. D. cross-section

Fig.6. Deformed structures and dislocation configuration of Ni20Cr wire with engineering

strain 46.6% in the T. D. cross-section

Fig.7. SAED patterns and deformation twin of Ni20Cr wire with engineering strain 36.1% in

the T. D. cross-section